

CONTOUR REGULARIZED LEFT VENTRICULAR STRAIN ANALYSIS FROM CINE MRI

Wei Feng, Thomas S. Denney Jr.

Steven Lloyd, Louis Dell'Italia, Himanshu Gupta

ECE Department
Auburn University
Auburn, AL USA

Division of Cardiovascular Disease
Univ. of Alabama at Birmingham
Birmingham, AL USA

ABSTRACT

Quantitative measurements of left ventricular (LV) strain are important in the diagnosis and management of patients with heart disease and tracking the efficacy of treatments over time. Tagged cardiac magnetic resonance imaging (MRI) is an established method for non-invasively measuring LV strains and strain rates, but non-tagged (or cine) MRI is the most commonly-used cardiac MRI protocol. In this paper, we propose a new algorithm for computing 2-D strains and strain rates from cine MRI that incorporates information from contours drawn at end-diastole and end-systole. These contours are typically drawn anyway at many institutions to compute LV volumes and contain important information on heart's deformation. Validation results on 18 normal human volunteers and 20 patients with myocardial infarction show good agreement between strains computed from cine MRI and those computed from tagged MRI using HARP analysis. Further validation on 45 patients with hypertension demonstrate that diastolic strains computed from cine MRI can measure changes in diastolic function common in hypertensive patients.

Index Terms— nonrigid registration, MRI, strain, left ventricle

1. INTRODUCTION

Quantitative measurements of left ventricular (LV) strain are important in the diagnosis and management of patients with heart disease and tracking the efficacy of treatments over time. Tagged cardiac magnetic resonance imaging (MRI) [1], [2] and related methods [3]–[5] are established methods for non-invasively measuring LV strains and strain rates. In tagged MRI, the myocardium is tagged before imaging with a spatially-encoded pattern that moves with the tissue. This pattern introduces contrast changes inside the myocardium that can be analyzed to measure strains and strain rates.

Non-tagged (or cine) MRI, however, is the most commonly-used cardiac MRI protocol. LV contours drawn on cine MR images are routinely used to measure global parameters of cardiac function such as LV volumes, diameters, and ejection fraction.

Estimates of LV strains and strain rates computed from cine MRI would have several advantages. First, cine MRI is more widely used and more accepted in the clinical community than tagged MRI. Also, tag patterns fade with time, and strains can become unreliable in late diastole. Measures of diastolic function, however, is important, particularly in patients with heart failure. While cine MRI lacks the increased myocardial contrast of tagged MRI, there are no major changes in signal intensity over time. Diastolic strain can be measured just as easily as systolic strain. Finally, reliable measures of radial strain are difficult with tagged MRI because the tag pattern sparsely samples myocardial motion in the radial direction. In cine

MRI, however, motion is primarily estimated from the spatiotemporal intensity changes near the endocardial (inner) and epicardial (outer) boundaries of the LV, which can potentially yield reasonable estimates of radial strain.

Several techniques have been proposed for computing 3-D strain from cine MRI [6]–[8] and have shown good results in a limited number of human studies or in animals where the subject is anesthetized and respiratory cycle is externally controlled. Slices in human cardiac cine MRI are most often acquired in different breath-holds, and registration errors between slices are common. While these registration errors can sometimes be corrected, they add an additional level of complexity to the algorithm and potential error to the result.

In this paper, we propose an algorithm for computing 2-D strain and strain rate from cine MRI based on non-rigid registration. While 2-D processing may seem like a step backward from 3-D methods, they are not affected by breath-hold registration errors. This is a particularly important feature in a clinical setting where patients with heart disease often have trouble holding their breath in a consistent position from slice to slice and registration errors are more common.

Non-rigid registration has been used to measure cardiac deformation in other modalities such as ultrasound [9], CT [10], and tagged MRI [11], [12], but these modalities have signal characteristics that are quite different than cine MRI. In [7], nonrigid registration was regularized by a constraint derived from continuum mechanics. Similarly, mechanical properties was also used to define deformation models in [8], where the registration was based both on the image data and shape features extracted from contouring of each slice and timeframe.

In this paper, a new non-rigid registration method is presented that incorporates user-drawn contours at ED and ES. These contours are usually drawn anyway to compute LV volumes and contain useful information that is incorporated into the strain computation. The motion is estimated in a two-stage process. In the first stage, non-rigid registration [13] is used to compute an interframe deformation field between timeframes. The interframe deformation fields are then used to propagate the ED and ES contours to all other timeframes [14]. In the second stage, the interframe deformation fields are refined by re-registering the images with a regularization term based on the propagated contours. Finally strains are computed from the refined motion estimate.

This paper is organized as follows. The strain computation algorithm is developed in Section 2. In Section 3, the strains and strain rates computed from cine MRI are compared to strains and strain rates computed from tagged MRI in the same patients using HARP analysis [15] and 3-D model-base analysis [16]. In Section 4, the results of a study are presented where cine MRI strains were computed in 38 normal human volunteers and 45 patients with hypertension. This preliminary study shows that the cine strains can detect

This work was supported by NIH grant P50-HL077100.

changes in strains and strain rates that have been reported in these two groups.

2. METHODS

2.1. Nonrigid Image Registration

In this paper, non-rigid registration is performed with an intensity-based sum of squared difference (SSD) similarity measure and a parametric deformation model [13]. Although mutual information based image registration algorithms perform well for inter-modal registration, SSD is an appropriate choice because tissues in cine MRI images have relatively consistent intensity values throughout the cardiac cycle. The interframe deformation is modeled with low resolution (compared to the image resolution) B-splines, which intrinsically regularize the solution. Gradient information presented around the myocardial wall, blood pool and papillary muscles drives the registration in adjacent low-gradient areas.

The registration cost function is defined as follows. In the two images to be registered, the image whose samples are fixed on regular grid throughout the registration is called the template image I_t . The other image which will be arbitrarily sampled according to the estimated deformation is called the source image I_s . Let

$$\mathbf{u}(\mathbf{t}; \boldsymbol{\mu}) = \sum_{i=1}^n \mu_i \beta^2 (\mathbf{t} - \mathbf{c}_i)$$

be the B-spline represented deformation at arbitrary point \mathbf{t} , where n is the number of control points used and \mathbf{c}_i is the location of control point i . The displacement at \mathbf{t} is then defined as

$$\mathbf{h}(\mathbf{t}; \boldsymbol{\mu}) = \mathbf{t} + \mathbf{u}(\mathbf{t}; \boldsymbol{\mu}).$$

The cost function is formulated as

$$J(\boldsymbol{\mu}) = \sum_{\mathbf{t}_k \in \Omega} [I_t(\mathbf{t}_k) - I_s(\mathbf{h}(\mathbf{t}_k; \boldsymbol{\mu}))]^2, \quad (1)$$

where the samples \mathbf{t}_k are taken from Ω , the set of sampling locations in the template region of interest (ROI). This optimization problem is solved using the Levenberg algorithm [17], which utilizes both the gradient and the Hessian of J .

To avoid local minima and reduce computational cost, multi-resolution iterative registration is employed. Cubic B-spline image interpolation is used in each iteration to reduce interpolation artifacts. Quadratic B-splines are used to model the inter-frame motion. The number of control points in the motion field model is adjusted in each resolution layer from coarse to fine to increase final registration accuracy. Note that the use of cubic and quadratic B-splines generates a twice differentiable cost function, which makes it possible to calculate explicitly not only gradient, but also Hessian of the cost used in optimization.

2.2. Contour Propagation

Contours are automatically propagated from the ED and ES timeframes to all other timeframes in the sequence using a modified version of the method presented in [14]. Propagating both ED and ES contours is more reliable than only propagating ED contours because the user defines the boundary between papillary muscles and the LV wall at ES. The algorithm works as follows. Given two adjacent time frames in a cine sequence, the template is registered to the source image as described in Section 2.1. Both ED and ES frames are used as starting templates, and the other frames are registered in a consecutive fashion. For example, consider a hypothetical setting of 20 total

frames with frames 1 and 8 being ED and ES respectively. In systole, [14] registers 1 and 2, then 2 and 3, 3 and 4, and so forth until 7 and 8 in the forward direction. Then the same pairs are registered again in the backward direction, i.e., 8 and 7, 7 and 6, and so forth until 2 and 1. The same procedure is also applied to diastole. During the course of registration, contours at ED and ES are propagated consecutively to all other frames. Since this is a two-way propagation, two sets of propagated contours are obtained from ED and ES. They are then combined with weights determined by their relative distances from ED and ES.

2.3. Contour-Regularized Image Registration - Refinement

Once the contours are propagated to all frames, the motion from first-stage registration is refined by adding the propagated contours as a regularization term in the image registration cost function (1). A contour image is created for both the template and source images from the contours. The contour-image intensity at point x is given by

$$I^c(x) = r \sum_{\text{endo, epi}} \exp\left(-\frac{d^2(x)}{2\sigma^2}\right), \quad (2)$$

where $d(x)$ is the distance from the endocardial and epicardial contours and σ is a parameter that controls the spread of the contours. $\sigma = 1$ pixel was used in all experiments. The scaling factor r is chosen such that the constructed contour images match up with the dynamic range of the template and source images. For example, if the dynamic range of both the template and the source images is $(0, 50)$, then $r = 50$.

Assuming $I_t^c(x)$ and $I_s^c(x)$ are the contour images for template and source, the contour-regularized cost function is

$$J_c(\boldsymbol{\mu}) = (1 - \lambda) \sum_{\mathbf{t}_k \in \Omega} \left([I_t(\mathbf{t}_k) - I_s(\mathbf{h}(\mathbf{t}_k; \boldsymbol{\mu}))]^2 \right) + \lambda \sum_{\mathbf{t}_k \in \Omega} \left(\lambda [I_t^c(\mathbf{t}_k) - I_s^c(\mathbf{h}(\mathbf{t}_k; \boldsymbol{\mu}))]^2 \right) \quad (3)$$

which is optimized in the same way as (1). Note that λ controls the overall impact of the contour regularization term. $\lambda = 0.5$ would put the same weight on matching of the contours as matching of the images. $\lambda = 0.1$ was used in all experiments. The effect of varying λ is studied in Section 3.1.

2.4. Strain Analysis from Motion

Once a refined interframe deformation field is estimated by optimizing (1), 2-D Lagrangian strain is computed as follows. Let $\mathbf{x}(t_i)$ be the spatial point at time t_i , $i = 1, 2, \dots$, and let \mathbf{u}_i be the motion field from t_i to t_{i+1} . Strain is computed in each frame by combining the accumulated inter-frame deformations. Starting from ED, denote any material point in the myocardium as \mathbf{X} . Let \mathbf{x}_n be the spatial point of \mathbf{X} at frame n . The forward displacement gradient tensor for \mathbf{X} at frame $n + 1$ can be derived as

$$F_{fw}^n = \prod_{i=1}^n \left(\frac{d\mathbf{u}_i(\mathbf{x}_i)}{d\mathbf{x}_i} + I \right) \quad (4)$$

The backward displacement gradient F_{bw}^n can be computed similarly. To reduce error accumulation, the forward and the backward propagated displacement gradients are combined using weights, w , determined by their relative distances from ED and ES:

$$F_n = wF_{fw}^n + (1 - w)F_{bw}^n.$$

Finally, the Lagrangian strain tensor at \mathbf{X} is computed as $E_n = (F_n^T F_n - I)/2$. The strain rate tensor was computed from the strains in each timeframe by a centered difference.

3. EXPERIMENTS

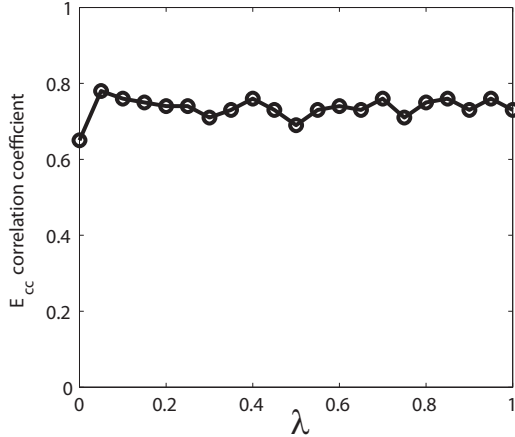


Fig. 1: Correlation coefficient between mid-ventricular circumferential strain (E_{cc}) computed from cine MRI and tagged MRI using HARP analysis for different values of the contour regularization parameter (λ). Correlation computed over training data.

3.1. Comparison with Tagged MRI and HARP

In this section, strains computed from cine data are compared with strains computed from tagged cardiac MRI.

38 normal human volunteers and 42 patients with myocardial infarction (MI) were scanned with both standard cine and tagged MRI. Circumferential and radial strains and strain rates were computed from the cine data with the algorithm described above, which was implemented in MATLAB. Approximately 7 minutes per study were needed to propagate contours and another 7 minutes was needed to refine the interframe deformations on a 2.6 GHz dual-core personal computer with 4 Gb of RAM. The same strains were computed from the tagged data using 2-D HARP analysis [15] and 3-D model-based analysis [16].

To evaluate the effect of λ , 20 normal and 20 MI patients were randomly selected. Strains were computed from the cine data with different values of λ . The results are shown in Fig. 1. $\lambda = 0$ corresponds to the case where contour-based regularization was not used to refine the interframe deformation. Increasing values of λ reflect an increasing influence of the contour term in (3) on the result. The correlation coefficients are consistently higher when $\lambda > 0$, which means that using contour-based regularization improves the quality of the strain estimates. Once contour-based regularization is used, however, the strain estimates are relatively insensitive to λ .

Based on the above observation, we chose $\lambda = 0.1$ and evaluated our algorithm on another set of 38 studies (18 normals and 22 MI patients) by comparing to both 3-D model-based analysis [18] and HARP. The correlation coefficient between mid-ventricular end-systolic circumferential strain (E_{cc}) computed from cine MRI and tagged MRI with 3-D model-based analysis was good ($\rho=0.83$).

The correlation coefficients between cine MRI and HARP E_{cc} , systolic E_{cc} rate, and early diastolic E_{cc} rate were 0.84, 0.73, and 0.61, respectively. The reduced correlation in systolic E_{cc} rate is most likely because tagged MRI introduces contrast inside the myocardium whereas, in cine MRI, deformation must be estimated primarily from the deformation of the myocardial boundaries. This is also true in early diastole, but the contrast in tagged MRI has faded considerably by this point. In cine MRI, however, myocardial boundary contrast is relatively constant throughout the cardiac cycle. The early diastolic E_{cc} rate computed from cine MRI may indeed be superior to that computed from tagged MRI, but more analysis is needed to support this claim.

Fig. 2a shows both cine and HARP mid-ventricular E_{cc} versus normalized time averaged over the 18 normal human volunteers. Time was normalized so that zero corresponds to end-diastole and 100 corresponds to peak early diastolic circumferential strain. The curves are fairly close together, with the exception of the inferior wall where cine MRI tends to over-estimate strain. Fig. 2b shows the same type of curve for radial strain (E_{rr}). The cine-based algorithms consistently estimates higher radial strains than HARP. Tagged MRI, however, is known to produce poor estimates of radial strain. The peak cine-MRI E_{rr} , however, is closer to wall thickness measurements in these subjects ($61 \pm 2.6\%$). This result suggests that the cine-MRI strain may be a more accurate estimate of radial strain than those computed from tagged MRI.

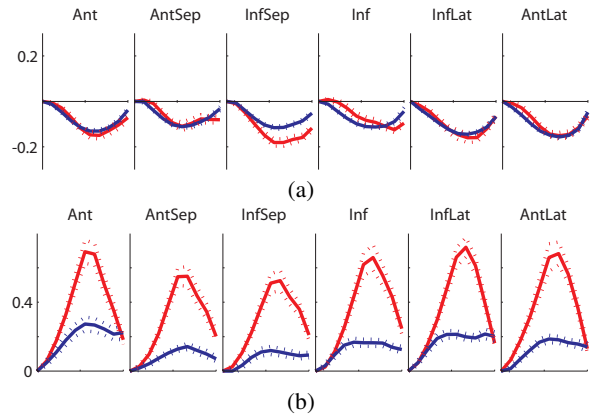


Fig. 2: Mid-ventricular circumferential (a) and radial (b) strains versus time computed from cine MRI (red) and tagged MRI/HARP (blue). Time normalized to the range 0 (end-diastole) to 100 (early diastole). The curves represent an average (solid) and \pm standard error (dotted) over 18 normal human volunteers.

3.2. Preliminary Study of Hypertension

In cine data, strains can be measured during diastole. In tagged MRI, the tag pattern fades with time and measurements of strain during diastole are often unreliable - particularly in late diastole when the left atrium contracts. Consequently, to validate the cine strains in diastole, strains were computed from standard cine MRI scans of 39 normal human volunteers and compared to 45 patients with hypertension. Patients with hypertension often have diastolic dysfunction. Diastolic dysfunction occurs when the heart wall becomes stiff, and the LV filling rate is reduced. In normals, filling mostly occurs during passive relaxation of the ventricle in early diastole. In patients

with diastolic dysfunction, however, early diastolic filling is reduced and more filling occurs during the atrial contraction phase.

Figure 3. shows the early and atrial diastolic circumferential expansion rates in both normals and hypertensive patients. In early diastole, circumferential expansion in hypertensives is lower than normal. In atrial diastole, circumferential expansion is higher than normal. This observation of early to atrial reversal in hypertensive patients is consistent with clinical measurements of mitral-valve inflow rates with Doppler ultrasound [19].

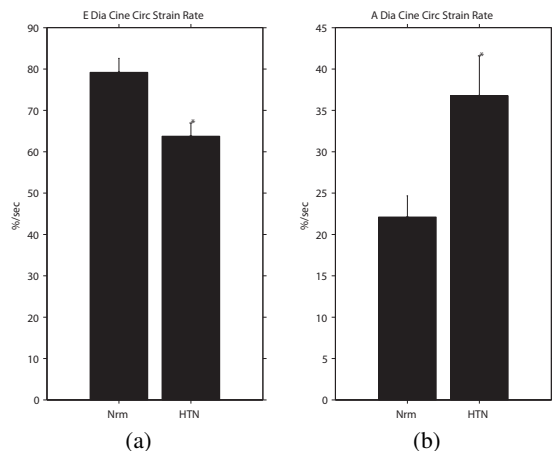


Fig. 3: Circumferential expansion rates in early (a) and atrial (b) diastole in normal human volunteers (Nrm) and patients with hypertension (HTN). * $P < 0.05$ vs. normal.

4. CONCLUSION

In this paper, a method was presented for measuring strains in standard cine MRI data. Circumferential strains computed from cine MRI correlate well with strains from tagged MRI during systole, and cine strains may be more accurate during diastole. Also radial strains computed from cine MRI may be more accurate than radial strain computed from tagged MRI over the entire cycle. Finally, strain from cine MRI may be more useful clinically, because cine MRI is more widely used in this environment.

In future work, we plan to further validate cine strains by comparison with other modalities such as Doppler ultrasound. We also plan to investigate ways to reduce the computation time needed to perform the contour propagation and interframe deformation refinement.

5. REFERENCES

- [1] E. Zerhouni et al., "Human heart: tagging with MR imaging – a method for noninvasive assessment of myocardial motion," *Radiology*, vol. 169, no. 1, pp. 59–63, 1988.
- [2] L. Axel and L. Dougherty, "Heart wall motion: improved method of spatial modulation of magnetization for MR imaging," *Radiology*, vol. 172, no. 2, pp. 349–360, 1989.
- [3] P. Selskog et al., "Kinematics of the heart: strain-rate imaging from time-resolved three-dimensional phase contrast MRI," *IEEE Transactions on Medical Imaging*, vol. 21, no. 9, pp. 1105–1109, Sep. 2002.

- [4] B. Spottiswoode et al., "Tracking myocardial motion from cine DENSE images using spatiotemporal phase unwrapping and temporal fitting," *IEEE Transactions on Medical Imaging*, vol. 26, no. 1, pp. 15–30, Jan. 2007.
- [5] J. Garot et al., "Spatially resolved imaging of myocardial function with strain-encoded MR imaging after myocardial infarction," *Radiology*, vol. 233, no. 3, pp. 596–602, Nov. 2004.
- [6] A. Bistoquet et al., "Left ventricular deformation recovery from cine MRI using an incompressible model," *IEEE Transactions on Medical Imaging*, vol. 26, no. 9, pp. 1136–1153, Sep. 2007.
- [7] A. Veress et al., "Measurement of strain in the left ventricle during diastole with cine-MRI and deformable image registration," *Journal of Biomechanical Engineering*, vol. 127, no. 7, pp. 1195–1207, December 2005.
- [8] A. Sinusas et al., "Quantification of 3-D regional myocardial deformation: shape-based analysis of magnetic resonance images," *American Journal of Physiology - Heart and Circulatory Physiology*, vol. 281, no. 2, pp. H698–H714, 2001.
- [9] M. Ledesma-Carbayo et al., "Spatio-temporal nonrigid registration for ultrasound cardiac motion estimation," *IEEE Transactions on Medical Imaging*, vol. 24, no. 9, pp. 1113–1126, Sep. 2005.
- [10] X. Papademetris et al., "Estimation of 3-D left ventricular deformation from medical images using biomechanical models," *IEEE Transactions on Medical Imaging*, vol. 21, no. 7, pp. 786–800, Jul. 2002.
- [11] N. Tustison and A. Amini, "Biventricular myocardial strains via nonrigid registration of anfigatomical NURBS models," *IEEE Transactions on Medical Imaging*, vol. 25, no. 1, pp. 94–112, Jan. 2006.
- [12] R. Chandrashekara et al., "Analysis of 3-D myocardial motion in tagged MR images using nonrigid image registration," *IEEE Transactions on Medical Imaging*, vol. 23, no. 10, pp. 1245–1250, Oct. 2004.
- [13] J. Kybic and M. Unser, "Fast parametric elastic image registration," *IEEE Transactions on Image Processing*, vol. 12, no. 11, pp. 1427–1442, Nov. 2003.
- [14] W. Feng et al., "Myocardial contour propagation in cine cardiac MRI," *Joint Annual Meeting ISMRM-ESMRMB*, p. 766, May 2007.
- [15] N. Osman et al., "Imaging heart motion using harmonic phase MRI," *IEEE Transactions on Medical Imaging*, vol. 19, no. 3, pp. 186–202, Mar. 2000.
- [16] J. Li and T. Denney Jr., "Left ventricular motion reconstruction with a prolate spheroidal b-spline model," *Physics in Medicine and Biology*, vol. 51, no. 3, pp. 517–537, 2006.
- [17] K. Levenberg, "A method for the solution of certain non-linear problems in least squares," *The Quarterly of Applied Mathematics*, vol. 2, pp. 164–168, 1944.
- [18] Jin Li and Thomas S Denney, "Left ventricular motion reconstruction with a prolate spheroidal b-spline model," *Phys Med Biol*, vol. 51, no. 3, pp. 517–537, Feb 2006.
- [19] Redfield et al., "Burden of systolic and diastolic ventricular dysfunction in the community: appreciating the scope of the heart failure epidemic," *JAMA*, vol. 289, no. 2, pp. 194–202, Jan 2003.